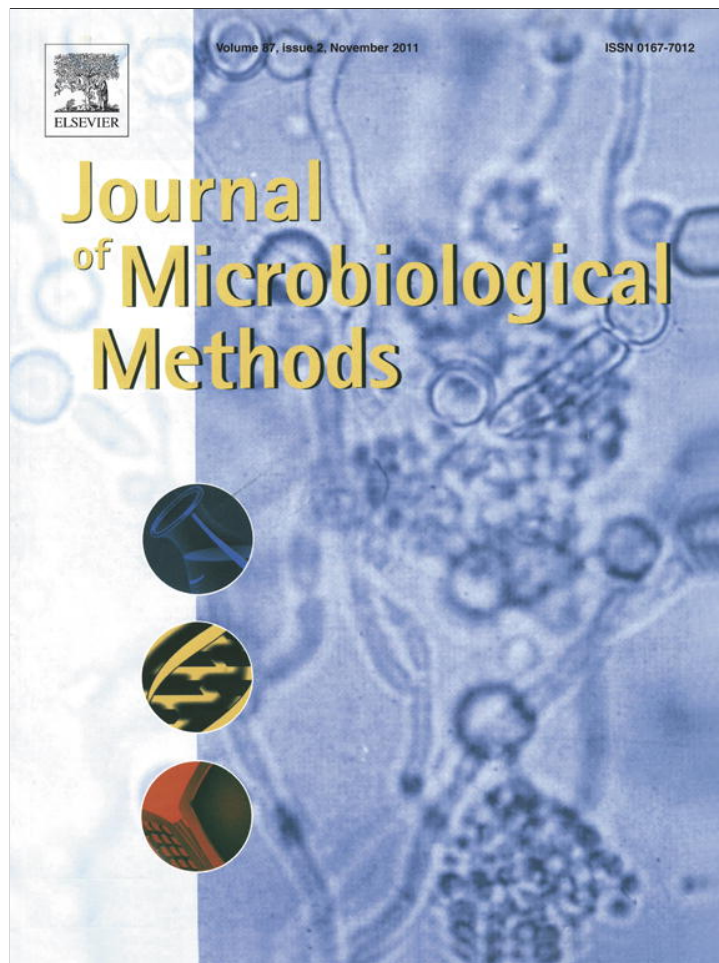


Provided for non-commercial research and education use.
Not for reproduction, distribution or commercial use.



This article appeared in a journal published by Elsevier. The attached copy is furnished to the author for internal non-commercial research and education use, including for instruction at the authors institution and sharing with colleagues.

Other uses, including reproduction and distribution, or selling or licensing copies, or posting to personal, institutional or third party websites are prohibited.

In most cases authors are permitted to post their version of the article (e.g. in Word or Tex form) to their personal website or institutional repository. Authors requiring further information regarding Elsevier's archiving and manuscript policies are encouraged to visit:

<http://www.elsevier.com/copyright>



Contents lists available at SciVerse ScienceDirect

Journal of Microbiological Methods

journal homepage: www.elsevier.com/locate/jmicmethDevelopment of 3D architecture of uropathogenic *Proteus mirabilis* batch culture biofilms—A quantitative confocal microscopy approachG. Schlapp^{a,1}, P. Scavone^{a,b,1}, P. Zunino^a, S. Härtel^{b,*}^a Department of Microbiology, Instituto de Investigaciones Biológicas Clemente Estable, Avda. Italia 3318, Montevideo, Uruguay^b Laboratory for Scientific Image Processing (SIAN-Lab), Anatomy & Developmental Biology Program, Biomedical Neuroscience Institute (BNI), ICBM, Faculty of Medicine, University of Chile, Santiago, Chile

ARTICLE INFO

Article history:

Received 19 April 2011

Received in revised form 25 July 2011

Accepted 28 July 2011

Available online 12 August 2011

Keywords:

Bacterial biofilms

Quantitative confocal laser scanning microscopy

Proteus mirabilis

ABSTRACT

This work studies the development of the 3D architecture of batch culture *P. mirabilis* biofilms on the basis of morpho-topological descriptors calculated from confocal laser scanning microscopy (CLSM) stacks with image processing routines. A precise architectonical understanding of biofilm organization on a morpho-topological level is necessary to understand emergent interactions with the environment and the appearance of functionally different progeny swarmer cells. *P. mirabilis* biofilms were grown on glass coverslips for seven days on LB broth and subjected to *in situ* immunofluorescence. Confocal image stacks were deconvolved prior to segmentation of regions of interest (ROI) that identify individual bacteria and extracellular material, followed by 3D reconstruction and calculation of different morpho-topological key descriptors.

Results showed that *P. mirabilis* biofilm formation followed a five stage process: (i) reversible adhesion to the surface characterized by slow growth, presence of elongated bacteria, and absence of extracellular material, (ii) irreversible bacterial adhesion concomitant to decreasing elongation, and the beginning of extracellular polymer production, (iii) accelerated bacterial growth concomitant to continuously decreasing elongation and halting of extracellular polymer production, (iv) maturation of biofilm defined by maximum bacterial density, volume, minimum elongation, maximum extracellular material, and highest compaction, and (v) decreased bacterial density and extracellular material through detachment and dispersion. Swarmer cells do not play a role in *P. mirabilis* biofilm formation under the applied conditions. Our approach sets the basis for future studies of 3D biofilm architecture using dynamic *in vivo* models and different environmental conditions that assess clinical impacts of *P. mirabilis* biofilm.

© 2011 Elsevier B.V. All rights reserved.

1. Introduction

In most natural, clinical or industrial settings, bacteria are found predominantly as irreversibly adhered communities or so-called 'biofilms', rather than planktonic cells, but the majority of laboratory studies focus on the latter (Costerton et al., 1995). Biofilms are found on virtually every natural and man-made surface and frequently associate to nosocomial infections. Several authors have described biofilm development as a process with an initial attachment of cells to a surface and production of exopolysaccharides resulting in more firmly and irreversible bacterial attachment (Costerton et al., 2003; Davey and O'Toole, 2000). After that, maturation of biofilm architecture begins, which varies from smooth and confluent to rough and

uneven with tall cell clusters interweaved by fluid-filled channels (Klausen et al., 2003). Finally, detachment and dispersion of planktonic cells from the biofilm to colonize new areas (Davey and O'Toole, 2000; Stoodley et al., 2002).

Confocal Laser Scanning Microscopy (CLSM) and image analysis tools have contributed to a better visual understanding of static and dynamic biofilm architecture in recent years (Renslow et al., 2011). In order to identify biological key events during and after biofilm formation, we developed image processing algorithms to identify individual bacteria, swarmer cells, and extracellular matrix and quantify their morpho-topological properties with mathematical descriptors.

Proteus mirabilis is a Gram-negative bacteria that causes diverse opportunistic and nosocomial infections (Stamm et al., 1997), and is particularly associated with complicated urinary tract infections as those that occur in catheterized patients or individuals with structural abnormalities of the urinary tract (Warren et al., 1982). It is well known that *P. mirabilis* forms biofilms on the surface of urinary catheters, which can lead to serious consequences for the patient (Stickler et al., 1993). In the present study we characterize the formation of *P. mirabilis* biofilm structure grown on LB broth and glass coverslips for seven days with 3D

* Corresponding author at: Laboratorio de Procesamiento de Imágenes SIAN, Programa de Anatomía y Biología del Desarrollo, BNI, ICBM, Facultad de Medicina, Universidad de Chile, Independencia 1027, Santiago, Chile. Tel.: +56 2 978 6366; fax: +56 2 978 6368.

E-mail address: shartel@med.uchile.cl (S. Härtel).

¹ Both authors contributed equally to this paper.

morpho-topological descriptors derived with processing routines from CLSM and image stacks. Our approach establishes a reliable method to analyze 3D biofilm formation that will contribute to the future understanding emergent biochemical, mechanical, and clinical properties in the context of the architectonical organization of bacterial communities.

2. Materials and methods

2.1. Bacterial strain

We used a wild-type *P. mirabilis* strain (Pr2921) that has been previously characterized genotypically and phenotypically (Zunino et al., 2000, 2001, 2003).

2.2. Mice immunization and serum preparation

In order to produce a polyclonal anti-*P. mirabilis* serum, seven 8-week-old female CD-1 mice were subcutaneously immunized with a formaline-inactivated Pr2921 culture (Li et al., 2004). In the first immunization (day 1) inactivated bacteria suspended in PBS were mixed with Freund's complete adjuvant (1:1) and 0.3 ml of this emulsion were subcutaneously injected in each mice. For subsequent immunizations (days 14 and 28), Freund's incomplete adjuvant was used. At day 40, blood samples were taken from each mouse by submandibular vein puncture and serum was obtained. Serum reactivity was evaluated by performing a simple agglutination assay, mixing a 1/100 dilution of the serum with a Pr2921 culture aliquot on a slide (1:1) and incubating at room temperature for 10 min with agitation. Agglutination was seen under a scope light. An aliquot of the culture mixed with a 1/100 dilution of a pre-immune serum (obtained from the same animals prior to immunization) in PBS was used as a negative control. Mice were provided with food pellets and tap water *ad libitum*. All animal experiments were conducted in accordance with procedures authorized by the Bioethics Committee of IIBCE, Montevideo, Uruguay.

2.3. In vitro biofilm formation

Pr2921 was statically grown in Luria Bertani (LB) broth at 37 °C for 48 h and then 0.3 ml of this culture was used to inoculate fifty-milliliter tubes containing a sterile glass coverslip (Corning) and 30 ml of fresh LB broth. Biofilms were allowed to form up to seven days at 37 °C, without shaking. Coverslips were taken out at the appropriate time and biofilms were fixed with 4% paraformaldehyde in PBS for 20 min. Bacterial viability was tested using a triple staining (propidium iodide, fluorescein diacetate and Hoechst 33342) (Moyes, 2009).

2.4. In situ immunofluorescence

Fixed biofilms were subjected to *in situ* immunofluorescence following a method described by Gu et al. (2005) with some modifications. The entire procedure was performed in humid chambers at room temperature. Briefly, fixed biofilms were exposed to a non-permeabilization buffer (NP; 2% bovine serum albumin in PBS, 0.05 M NH₄Cl, pH 7.2) for 20 min. Then, covers were washed three times with PBS and incubated for 1 h with a 1/50 dilution of the polyclonal anti-Pr2921 serum (primary antibody) prepared in NP buffer. Covers were washed and exposed to a 1/100 dilution of an anti-mouse antibody (secondary antibody) conjugated to fluorescein isothiocyanate (FITC) in NP buffer for 30 min. Finally, covers were washed and put over microscope slides using 10 µl of a mounting solution. Covers were protected from light and subjected to CLSM observation immediately in order to preserve biofilm structure.

2.5. Image acquisition by CLSM

Acquisition of 3D image stacks was performed using an Olympus BX-61 FV300 CLS microscope, Fluoview software 4.3, a 100× oil immersion objective (NA = 1.35), and 488/520 nm excitation/emission wavelength. At least three z-stacks were randomly chosen in each sample, using an acquisition step size of 0.3 µm in the z-axis and 1024 × 1024 pixels in the xy-plane with a pixel size of 70 nm. The acquisition sampling rates in the xy-plane and the z-axis are close to the Nyquist criteria for the microscopic setup that have been calculated with Huygens Scripting Software (Scientific Volume Imaging, Hilversum, Netherlands).

2.6. Image processing and morpho-topological descriptors for biofilm architecture

3D image stacks were deconvolved with Huygens Scripting Software. The deconvolution parameter 'signal to noise ratio' was adjusted until the deconvolved images were free of pixel noise. All image-processing routines described below were developed in one of the authors laboratories (SCIAN-Lab, www.scian.cl) on the basis of IDL 7.0 (Interactive Data Language, ITT, CO, USA), including interactive tools for the segmentation of different regions of interest (ROIs), for visualization, 3D reconstruction, and determination of mathematical morpho-topological descriptors. We applied isotropic Laplace filters with a radius $r = 3$ for the segmentation of the bacteria. This operation presents a convolution of the original image $I(x,y)$ with a kernel $k: k[x,y] \otimes [x,y] = I'[x,y]$. The application of Laplace Kernels leads to homogeneous images $I'[x,y]$ across the xy-planes where regions without intensity gradients (background or plateaus) are convolved to zero. After convolution, thresholds values selected in $I'[x,y]$ define the bacterial borders across the images, and the regions within these borders were selected by operations according to size and morphology. Elements touching the image border were erased automatically. The second segmentation procedure defined bacteria together with associated extracellular material through a texture sensitive approach. To this end we applied the Scaling Index Method (Räth and Morfill, 1997), a pixel-wise non linear transformation in combination with a threshold value that we modified previously with a weighting vector (Härtel et al., 2005b). After the segmentation of individual bacteria and extracellular material; bacterial number, total bacterial volume, and bacterial and extracellular material volume were calculated directly from the ROI data. In order to evaluate the presence of swarmer cells in biofilms, elongation of bacteria was calculated as $[1 - (\text{width}/\text{length})]$ considering each bacteria surrounded by a 3D box model defined by the principal axis (Härtel et al., 2007). Microcolonies formation was characterized using a 2D model of distance, in which distance distributions were determined and bacteria sorted into 4 groups: $0 \leq d_1 \leq 210$ nm, $210 \text{ nm} < d_2 \leq 1.62$ µm, $1.62 \text{ µm} < d_3 \leq 2.4$ µm, and $2.4 \text{ µm} < d_4$. Microcolonies were defined by more than 8 cells within group d_1 . In addition, hexagonal lattice formation was quantified according to Härtel et al. (2005a). Finally, we analyzed the percentage of border pixels within a distance of 210 nm towards the adjacent border and classified the bacteria into groups that share 5–20%, and more than 30% with the nearest neighbors.

2.7. Data analysis

Duncan test (Statistica 7.0) was performed in order to compare values registered along time.

3. Results

3.1. In vitro biofilm formation, CLSM acquisition and segmentation of ROIs

Pr2921 *P. mirabilis* biofilms were statically grown on coverslips from one to seven days of incubation. Biofilms were successfully labeled with

a polyclonal anti-Pr2921 serum and *in situ* immunofluorescence. CLSM imaging of biofilms showed a consistent and clear FITC signal corresponding to the bacterial cell surface proteins, LPS and capsules independent of the incubation period (Fig. 1). Fig. 2A,B shows the result of deconvolution which presents a necessary step for reliable segmentation of individual bacteria and extracellular material (Fig. 2D,E). A negative labeling control in which biofilms were exposed to the immunofluorescence method but without exposition to the incubation serum showed no FITC signal (not shown). Adhesion reversibility of Pr2921 to coverslips was tested on biofilms grown after one and two days of incubation without fixation. We observed that bacteria grown on coverslips after 1-day incubation was easily removed with gently rinsing, showing a weaker and probably reversible adhesion. Meanwhile, bacteria showed an irreversible adhesion after two days of incubation. Bacteria remained viable along all the assay period according to the results of the triple staining analysis (data not shown).

3.2. Characterization of biofilm architecture by morphological descriptors

At day one, we counted a total number of 357 ± 68 bacteria per stack (mean \pm SE, $N = 3$), and the number increased successively until it reached a maximum value at day 5 (6925 ± 981). After day 5, we observed a decrease in the number of bacteria per stack (Fig. 3A). Statistical analysis showed that the increase in the number of bacteria was significant after 4 days of incubation and at later time points (Duncan test, $p < 0.05$). The analysis of the slope of the variation of bacterial number per stack suggested a division of the process into three phases (Fig. 3A): (I) the first phase (days 1–3), was characterized by a low number of adhered bacteria, (II) the second phase (days 4–5) showed an accelerated growth of the number of bacteria towards a maximum value at day 5, and (III) the third phase showed a decreasing bacterial density. The variation of total bacterial

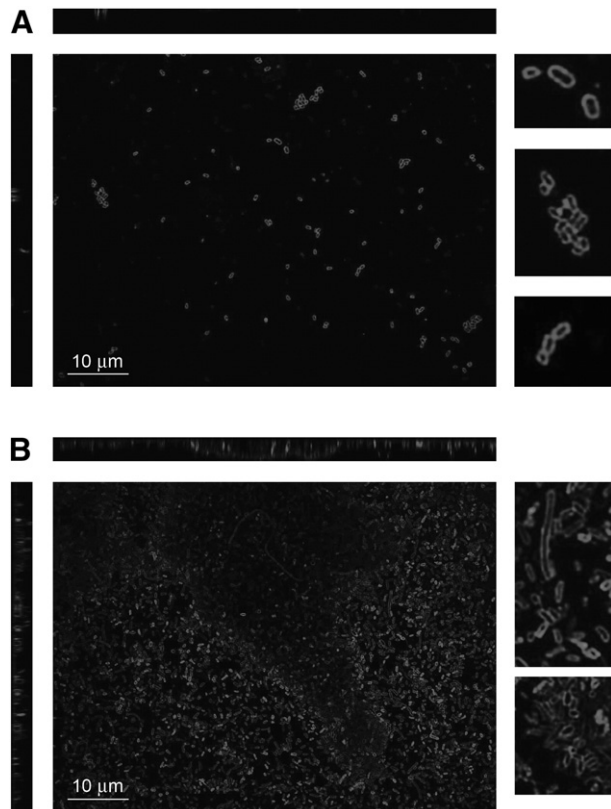


Fig. 1. A. CLSM stack of Pr2921 biofilm after 1-day incubation. B. Biofilm after 7-day incubation. In A and B, center images correspond to xy planes, upper images to xz planes, and left images to yz planes. Details in the right images are magnified 5 \times in respect to the center images. Scale bar represents 10 μ m.

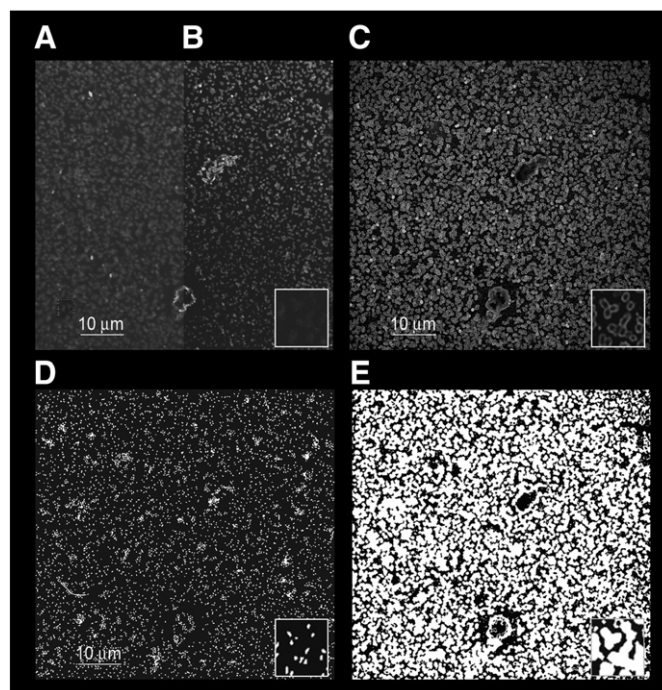


Fig. 2. Segmentation of individual bacteria and extracellular material by image processing. The CLSM stacks (A) were deconvolved (B) and subjected to Laplace filtering (C). Two types of segmentation were performed to distinguish individual bacteria (D) and bacteria and extracellular material (E). Details shown in the insets are magnified 3 \times in respect to the original images. Scale bar represents 10 μ m.

volume per stack during the 7-day incubation showed a similar behavior (Fig. 3B) with a significant increase at day 5 ($p < 0.05$). As before, the process was divided into three steps: (I) a constant increase in volume during the first 4 days, (II) a maximum value at day 5, and (III) a decrease in volume. Fig. 3C shows the sum of bacterial and extracellular material volume per stack which increased from days 2 to 3 and days 4 to 5, values on days 3 and 5 were significantly different from the previous ones ($p < 0.05$). Finally, the elongation of the bacteria showed a maximum value of ~ 0.6 at day 1 and decreased towards a plateau of ~ 0.4 at day 4 (Fig. 3D) ($p = 0.017$, $p = 0.033$ for days 1 and 2, respectively).

3.3. Characterization of biofilm architecture by topological descriptors

The distance model showed that small groups of bacteria defined by 8 neighbors (microcolonies) with a distance to the nearest neighbor ≤ 210 nm (d_1 group) were detected from the first day (Fig. 4B, red circles). As Fig. 4C shows, the hexagonal lattice model indicates increasing compactness until day 5, and the model maintained the typical pattern of a randomly seeded population (Härtel et al., 2005a; Fanani et al., 2010). Biofilm patches characterized by connected bacteria and extracellular material within d_1 group started to appear at day 5 within the pattern of the randomly seeded population. Finally, we show that the percentage of bacteria sharing between 5–20% of their surface did not change significantly with time (Fig. 5A), while the percentage of bacteria sharing more than 30% of its surface increased from days 5 to 7 (Fig. 5B).

The characteristics of the morphologic and topologic descriptors suggest the definition of a five step process for the formation and maturation of *P. mirabilis* biofilms on coverslips and LB broth: (i) reversible bacterial adhesion to the surface characterized by a slow growth, presence of elongated bacteria, and absence of extracellular matrix (day 1), (ii) irreversible bacterial adhesion concomitant to decreasing elongation, and the beginning of extracellular polymer production (days 2–3), (iii) accelerated bacterial growth concomitant

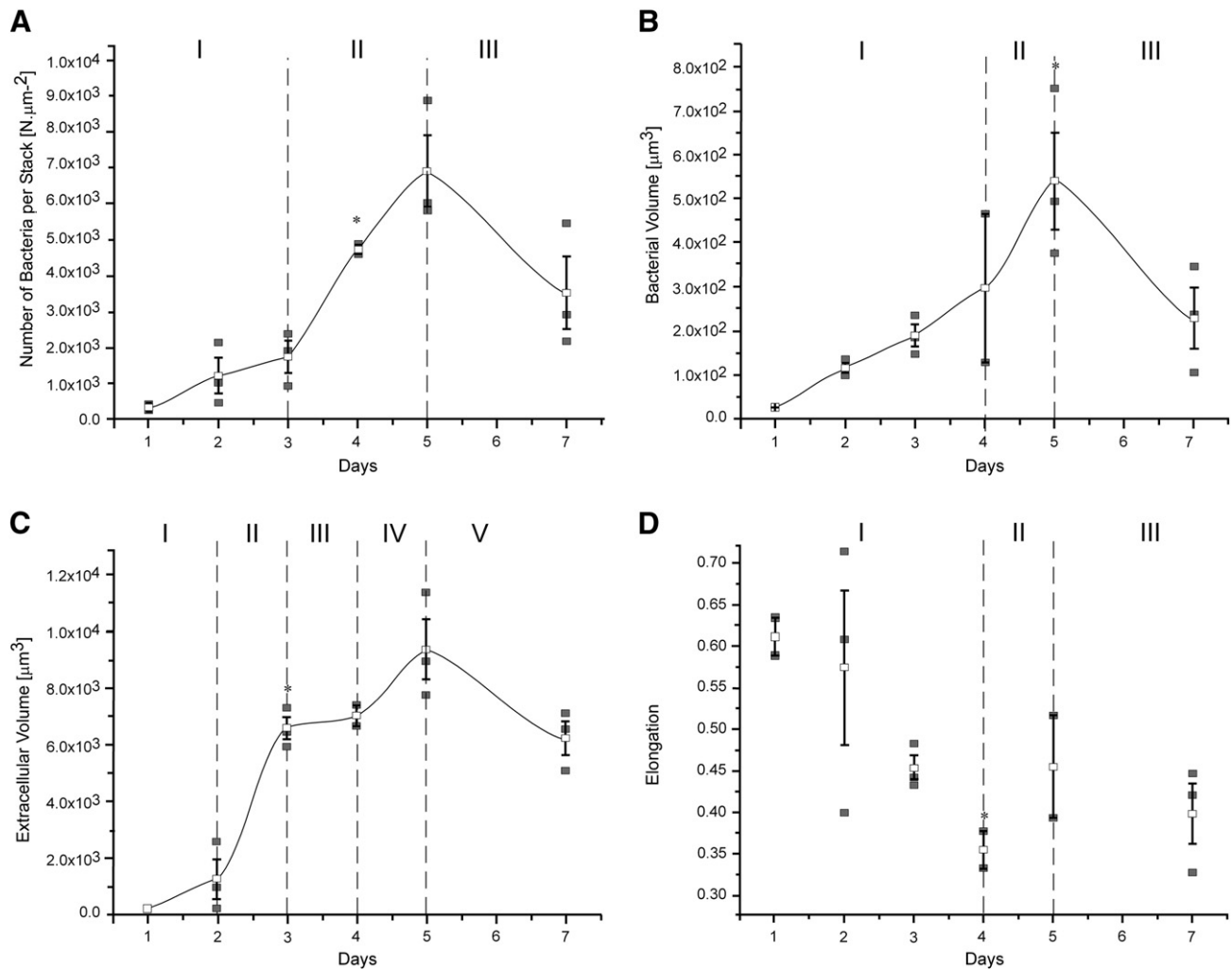


Fig. 3. Morphological features of growing biofilms. A. Number of bacteria per stack ($N \mu\text{m}^{-2}$). B. Total bacterial volume per stack (μm^3). C. Bacterial and extracellular material volume per stack (μm^3). D. Elongation of bacterial cells. White symbols represent mean values of $n = 3$ independent experiments (black symbols). Error bars represent standard errors and lines connect mean values by beta-splines.

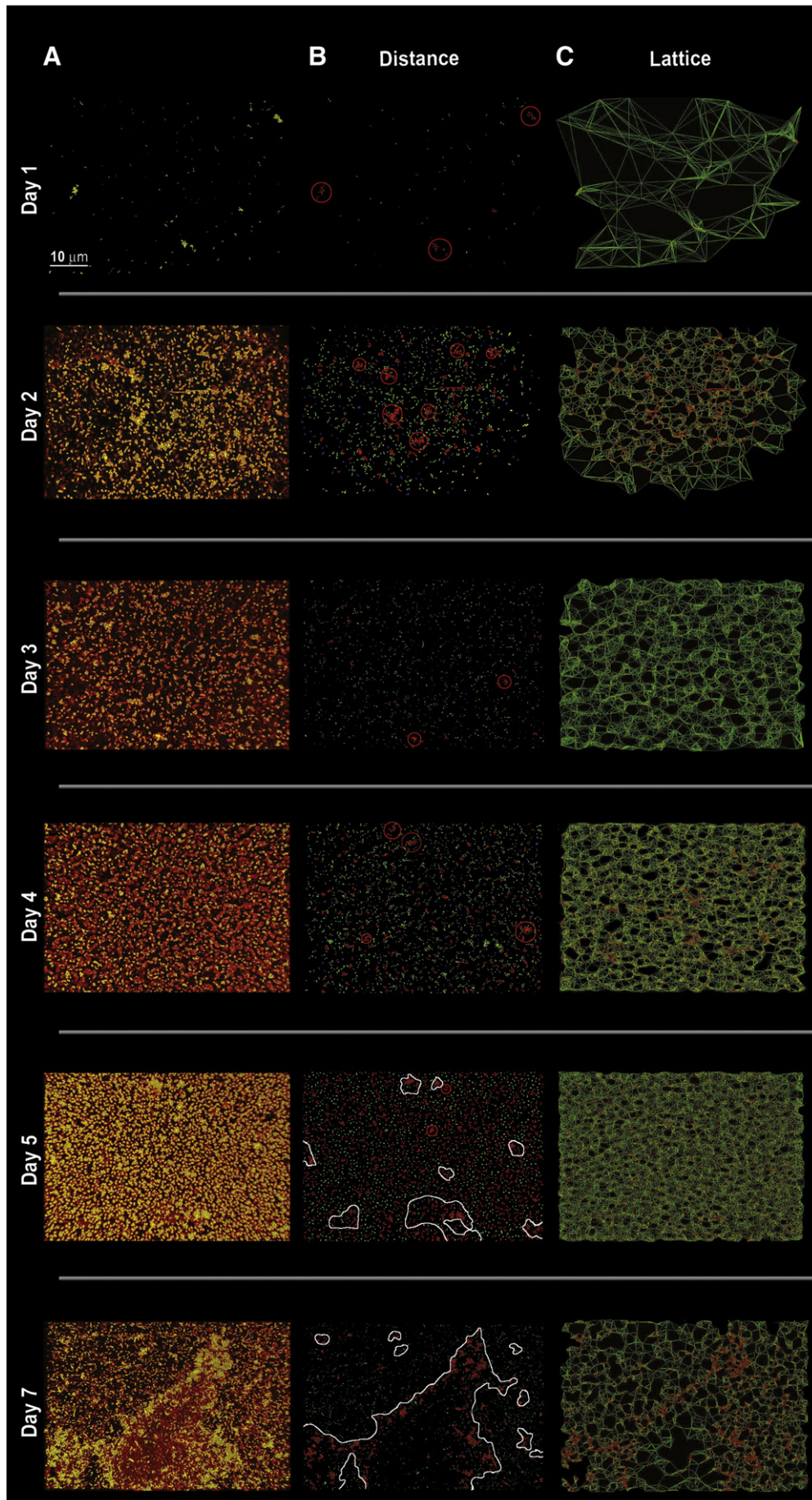
to continuously decreasing elongation and halting of extracellular polymer production (days 3–4), (iv) maturation of biofilm defined by maximum bacterial density, volume, minimum elongation, maximum extracellular material, and highest compaction (day 5), and (v) decreased bacterial density and extracellular material through detachment and dispersion (day 7). No mushroom-like structures were observed; under the applied condition, biofilm resulted to be flat with a maximum height of 2–3 bacteria (Fig. 1B).

4. Discussion

In this work, we characterize uropathogenic *P. mirabilis* biofilm formation process over glass coverslips in a close culture system. This first approach sets the basis for future studies of 3D biofilm architecture, using flowing culture systems and different environmental conditions to assess clinical impacts of *P. mirabilis* biofilm. The use of immunofluorescence based on a polyclonal anti-*P. mirabilis* mouse immune serum raised against whole *P. mirabilis* cells resulted in an appropriate technique for staining cells and cell products. The development of *P. mirabilis* biofilms was analyzed by CLSM, which allowed us to conduct non-invasive observations at single-cell resolution. In order to analyze and extract morpho-topological features, 3D CLSM stacks were deconvolved to lower Poisson noise to an imperceptible degree, prior to segmentation of the individual bacteria. The applied segmentation steps are critical for 3D biofilm

structure analysis, since they influence subsequent feature extraction in a direct manner (Yerly et al., 2007). Noise reduction and signal enhancement by deconvolution improves significantly when complementing information from the z-axis is provided and the xyz-voxel size during acquisition is close to the Nyquist criteria of diffraction limited microscopy. Unfortunately, this is not the case in most CLSM related studies on biofilm formation (Xavier et al., 2001; Yerly et al., 2007; Beyenal et al., 2004; Renslow et al., 2011). To minimize possible errors, sophisticated deconvolution software based on solid physical and probabilistic criteria should be preferred above simpler methods. Deconvolved images do not require any additional steps to improve signal noise ratio such as diffusion techniques suggested by Yerly et al., 2007. While diffusion techniques iteratively smooth the image data in regions without edges, deconvolution actually removes photon noise based on a probability criteria and the characteristics of the microscopic Point Spread Function (PSF), and should be applied to guarantee the best possible results for subsequent segmentation of bacteria borders, centers, and extracellular matrix.

It should be emphasized that most of the literature published in the field so far does not take into account the importance to work at the diffraction limit of confocal microscopy which requires sampling rates of approximately $50 \times 50 \times 150$ nm in the xyz dimensions (depending on the specific microscopic settings). In this context, Yerly et al. (2007) only defines the z-sampling distance (0.5 μm), the use of a 40 \times objective and an image size of 1024×1024 in the xy-plane which is insufficient to



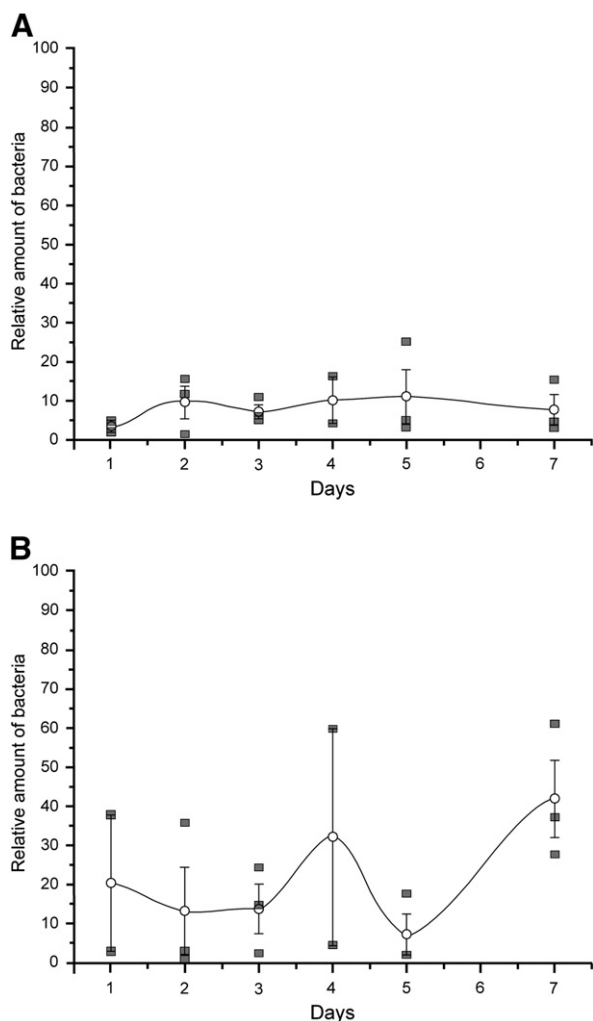


Fig. 5. 2D Neighborhood model during biofilm formation. A. Relative amount of bacteria sharing 5–20% of its surface with adjacent bacteria. B. Relative amount of bacteria sharing more than 30% of its surface with adjacent bacteria. White symbols represent mean values of $n=3$ independent experiments (black symbols). Error bars represent standard errors and lines connect mean values by beta-splines.

deduce the pixel size (zoom-dependence). Renslow et al. (2011) address the very interesting question of biofilm image reconstruction from structural data of the film, but never inform the xyz dimension of their model. Finally, Xavier et al. (2001) introduced their “Objective Threshold Selection” procedure for image data sampled by $624 \times 624 \times 2000$ nm in the xyz dimensions. Sampling rates beyond the Nyquist frequency affect the spatial relation between photon noise (always pixel size) and the full width at half maximum value of the microscopic PSF fluorescent point sources (in the range of 200–300 nm). In consequence, segmentation procedures that depend on signal/noise characteristics and structural parameters of the biofilm that depend on the resolution of the biofilm border at the interphase with the medium (such as fractal dimension and perimeters) might depend on the chosen sampling size. On the other hand, sampling rates close to the Nyquist frequency assure the best possible noise reduction, the best possible quantification of perimeters and related parameters such as

curvatures or fractal dimension, and comparable results among different laboratories that work at the diffraction limit.

There is some debate among researchers regarding the appropriate method for biofilm segmentation (e.g. Xavier et al., 2001; Baveye, 2002; Merod et al., 2007; Yerly et al., 2007). Although automatic techniques have been proposed for biofilm image analysis, we prefer to combine background knowledge and expertise with visual control of the results to guarantee a reliable segmentation. In order to circumvent the problem of heterogeneous sample illumination that cannot always be avoided, we have excellent experience with Laplace filters. Laplace filters with an adaptable kernel size set noise free background or intensity plateaus to zero and enhance point sources or membrane regions of individual bacteria across the xy-plane which can be segmented by thresholds afterwards. The filling of closed binary membrane regions leads to a uniform segmentation of the bacterial cytoplasm across the images. Segmentation results were vigorously checked by consecutive overlay of the segmented and the original images by different researchers. Previously to this work, segmentation based on Laplace filters after noise reduction through deconvolution has provided excellent results for the identification of mitochondria in cardiomyocytes (Parra et al., 2008), or GABA_B receptors, Golgi/Golgi-outposts, and ER in neuronal dendrites (Ramirez et al., 2010, 2011). Fluorescent staining of membranes of subcellular organelles such as mitochondria, Golgi/Golgi-outposts, or ER in combination with microscopic imaging at the diffraction limit yields image characteristics which are very similar to those of the bacteria shown in Figs. 1 and 2.

Biofilm formation and architecture can vary between different bacteria or culture conditions. Tolker-Nielsen and Molin (2000) proposed that every microbial biofilm community is unique although some structural attributes can be considered in universal terms. For example, CLSM data published by Jones et al. (2007) showed that *P. mirabilis* biofilms in LB formed a mushroom-like architecture while biofilms grown in urine formed a flat layer. The structural difference was probably due to nutrient deprivation which could also explain the flat layer biofilm observed during the 7-day incubation in this work. When bacterial elongation was measured to evaluate the possible contribution of swarmer cells to *P. mirabilis* biofilm formation, we observed that the average cellular length decreased in time. Therefore, we exclude the contribution of swarmer cells in biofilm formation during the 7-day incubation period for static growth on coverslips with LB broth.

Measures of different parameters obtained from CLSM images revealed that the number of bacteria, bacterial volume, and volume of extracellular matrix progressively increased until day 5, concomitant to the increasing compaction until the formation of large scale patches between days 5 and 7. Using the neighborhood model, microcolonies were detected from day 1 which distributed without any recognizable pattern within the culture (d_1 -group with $n>8$), and we determined that the amount of bacteria sharing more than 30% of their surface increased between days 5 and 7 which is in line with the observation of densely packed bacteria at the border of the large scale patches (especially day 7). The observation of densely packed bacteria at the border of the large scale patches which provide abundant extracellular material are in line with the suggested role of the matrix acting as a structural scaffold and a protective barrier against deleterious substances (Parsek and Tolker-Nielsen, 2008; Tolker-Nielsen and Molin, 2000). There are several bactericidal factors and secreted inhibitors of bacterial adherence in urine that naturally interfere with bacterial survival and multiplication (Agace et al., 1996), hence the

Fig. 4. Models of biofilm formation from days 1 to 7. A. 3D Stacks of bacteria were colored in yellow and extracellular material in red and protected onto a 2D plane. B. 2D Distance model: distances between bacteria were calculated and sorted into four groups: $0 \leq d_1(\text{red}) \leq 210$ nm; $210 \text{ nm} < d_2(\text{green}) \leq 1.62 \mu\text{m}$, $1.62 \mu\text{m} < d_3(\text{blue}) \leq 2.4 \mu\text{m}$, and $2.4 \mu\text{m} < d_4(\text{yellow})$. Microcolonies with 8 or more neighbors and distances ≤ 210 nm are outlined with red circles, patches with dense extracellular material are outlined by white lines. C. 2D Lattice model: the green lines represent the connection between each bacteria and its six closest neighbors. Scale bar represents $10 \mu\text{m}$ (first image, left).

extracellular matrix should play an important role in bacterial protection in biofilms.

In summary, our results evidence that *P. mirabilis* biofilms are generated through coordinated and well defined morpho-topological processes. We reported a first step towards a technique for the characterization of uropathogenic *P. mirabilis* biofilm formation at the diffraction limit of CLSM which leads to the best possible quantification of morpho-topological parameters through image processing algorithms. Biofilm characterization at the diffraction limit guarantees comparable results among laboratories which otherwise depend on the selected xyz-sampling rates. This approach will be essential to characterize the architecture of *P. mirabilis* biofilms grown in conditions that mimic urinary catheters (e.g. flow cells and urine as liquid medium) in the future, and to design strategies which avoid biofilm formation, particularly those associated to medical implants. In this context, we are presently carrying out experiments to assess the influence of diverse environmental factors and the role of different bacterial surface organelles on *P. mirabilis* biofilm formation.

5. Conclusions

We characterized the formation of batch culture *P. mirabilis* biofilms as a 7-day process which included reversible and irreversible bacterial adhesion, development of biofilm architecture in form of microcolonies, extracellular polymer production and densely packed bacteria at the border of large scale patches enriched with extracellular material. We can further exclude that swarmer cells play a role in *P. mirabilis* biofilm formation under the applied conditions, and present a reliable framework for future studies of 3D biofilm architecture using dynamic *in vivo* models as well as different environmental conditions which assess the clinical impact of *P. mirabilis* biofilm formation.

6. Abbreviations

CLSM	confocal laser scanning microscopy
FITC	fluorescein isothiocyanate
LB	Luria–Bertani (broth)
PSF	Point Spread Function
ROIs	regions of interest

Acknowledgments

The authors thank E. Labbe for support with the figures. Research in SCIAN-Lab (SH) is funded by FONDECYT (1090246), FONDEF (D0711019), and the Biomedical Neuroscience Institute (BNI, ICM P09-015-F). SCIAN-Lab is a selected member of the German–Chilean Center of Excellence Initiative (DAAD). P. Scavone is funded by International Biological Imaging Network (IBIN), PBCT ACT 47 and ANII-FCE 07-226 (Uruguay). G. Schlapp was funded by ANII Postgraduate Fellowship Program (Uruguay), and received a grant from PEDECIBA (Uruguay) to spend a short term fellowship in SCIAN-Lab.

References

- Agace, W., Connell, H., Svanborg, C., 1996. Host resistance. In: Mobley, H.L.T., Warren, J.W. (Eds.), *Urinary Tract Infections: Molecular Pathogenesis and Clinical Management*. American Society of Microbiology, Washington D.C.
- Baveye, P., 2002. Comment on: "Evaluation of biofilm image thresholding methods". *Water Res.* 36, 805–807.

- Beyenal, H., Donovan, C., Lewandowski, Z., Harkin, G., 2004. Three-dimensional biofilm structure quantification. *J. Microbiol. Methods* 59, 395–413.
- Costerton, J.W., Lewandowski, Z., Caldwell, D.E., Korber, D.R., Lappin-Scott, H.M., 1995. Microbial biofilms. *Annu. Rev. Microbiol.* 49, 711–745.
- Costerton, J.W., Veeh, R., Shirtliff, M., Pasmore, M., Post, C., Ehrlich, G., 2003. The application of biofilm science to the study and control of chronic bacterial infections. *J. Clin. Invest.* 112, 1466–1477.
- Davey, M.E., O'Toole, G.A., 2000. Microbial biofilms: from ecology to molecular genetics. *Microbiol. Mol. Biol. Rev.* 64, 847–867.
- Fanani, M.L., Härtel, S., De Tullio, L., Jara, J., Olmos, F., Oliveira, R., Maggio, B., 2010. The action of sphingomyelinase in lipid monolayers as revealed by microscopic image analysis. *Biochimica et Biophysica Acta (BBA) Biomembranes* 1798, 1309–1323.
- Gu, F., Lux, R., Du-Thumm, L., Stokes, L., Kreth, J., Anderson, M.H., Wong, D.T., Wolinsky, L., Sullivan, R., Shi, W., 2005. In situ and non-invasive detection of specific bacterial species in oral biofilms using fluorescently labeled monoclonal antibodies. *J. Microbiol. Methods* 62, 145–160.
- Härtel, S., Fanani, M.L., Maggio, B., 2005a. Shape transitions and lattice structuring of ceramide-enriched domains generated by sphingomyelinase in lipid monolayers. *Biophys. J.* 88, 287–304.
- Härtel, S., Rojas, R., Räh, C., Guarda, M.I., Goicoechea, O., 2005b. Identification and classification of di- and triploid erythrocytes by multi-parameter image analysis: a new method for the quantification of triploidization rates in rainbow trout (*Oncorhynchus mykiss*). *Arch. Med. Vet.* XXXVII 2, 147–154.
- Härtel, S., Jara, J., Lemus, C.G., Concha, M.L., 2007. 3D morpho-topological analysis of asymmetric neuronal morphogenesis in developing zebrafish. In: Tavares, J.M., Natal, J.R.M. (Eds.), *Computational Modelling of Objects Represented in Images. Fundamentals, Methods and Applications*. Taylor and Francis, Bristol (PA).
- Jones, S.M., Yerly, J., Hu, Y., Ceri, H., Martinuzzi, R., 2007. Structure of *Proteus mirabilis* biofilms grown in artificial urine and standard laboratory media. *FEMS Microbiol. Lett.* 268, 16–21.
- Klausen, M., Heydorn, A., Ragas, P., Lambertsen, L., Aaes-Jørgensen, A., Molin, S., Tolker-Nielsen, T., 2003. Biofilm formation by *Pseudomonas aeruginosa* wild type, flagella and type IV pili mutants. *Mol. Microbiol.* 48, 1511–1524.
- Li, X., Lockett, C.V., Johnson, D.E., Lane, M.C., Warren, J.W., Mobley, H.L.T., 2004. Development of an intranasal vaccine to prevent urinary tract infection by *Proteus mirabilis*. *Infect. Immun.* 72, 66–75.
- Merod, R.T., Warren, J.E., McCaslin, H., Wuertz, S., 2007. Toward automated analysis of biofilm architecture: bias caused by extraneous confocal laser scanning microscopy images. *Appl. Environ. Microbiol.* 73, 4922–4930.
- Moyes, R.B., 2009. Fluorescent staining of bacteria: viability and antibody labeling. *Curr. Protoc. Microbiol.* 15, A.3K.1–A.3K.13 (Appendix 3, Appendix 3K).
- Parra, V., Eisner, V., Chiong, M., Criollo, A., Moraga, F., Garcia, A., Härtel, S., Jaimovich, E., Zorzano, A., Hidalgo, C., Lavandero, S., 2008. Changes in mitochondrial dynamics during ceramide-induced cardiomyocyte early apoptosis. *Cardiovasc. Res.* 77, 387–397.
- Parsek, M.R., Tolker-Nielsen, T., 2008. Pattern formation in *Pseudomonas aeruginosa* biofilms. *Curr. Opin. Microbiol.* 11, 560–566.
- Ramirez, O.A., Garcia, A., Rojas, R., Couve, A., Härtel, S., 2010. Confined displacement algorithm determines true and random colocalization in fluorescence microscopy. *J. Microsc.* 239, 173–183.
- Ramirez, O.A., Härtel, S., Couve, A., 2011. Location matters: the endoplasmic reticulum and protein trafficking in dendrites. *Biol. Res.* 44, 17–23.
- Räh, C., Morfill, G., 1997. Texture detection and texture discrimination with anisotropic scaling indices. *J. Opt. Soc. Am. A* 14, 171–176.
- Renslow, R., Lewandowski, Z., Beyenal, H., 2011. Biofilm image reconstruction for assessing structural parameters. *Biotechnol. Bioeng.* 108, 1383–1394.
- Stamm, W.E., Martin, S.M., Bennett, J.V., 1997. Epidemiology of nosocomial infections due to gram negative bacilli: aspects relevant to development and use of vaccines. *J. Infect. Dis.* 136, 151–160 (Suppl.S).
- Stickler, D.J., Ganderton, L.J., King, J., Nettleton, J., Winters, C., 1993. *Proteus mirabilis* biofilms and the encrustation of urethral catheters. *Urol. Res.* 21, 407–411.
- Stoodley, P., Sauer, K., Davies, D.G., Costerton, J.W., 2002. Biofilms as complex differentiated communities. *Annu. Rev. Microbiol.* 56, 187–209.
- Tolker-Nielsen, T., Molin, S., 2000. Spatial organization of microbial biofilm communities. *Microb. Ecol.* 40, 75–84.
- Warren, J.W., Tenney, J.H., Hoopes, J.M., Muncie, H.J., Anthony, W.C., 1982. A prospective microbiologic study of bacteriuria in patients with chronic indwelling urethral catheters. *J. Infect. Dis.* 146, 719–723.
- Xavier, J.B., Schnell, A., Wuertz, S., Palmer, R., White, D.C., Almeida, J.S., 2001. Objective threshold selection procedure (OTS) for segmentation of scanning confocal laser microscopy images. *J. Microbiol. Methods* 47, 169–180.
- Yerly, J., Hu, Y., Jones, S.M., Martinuzzi, R.J., 2007. A two-step procedure for automatic and accurate segmentation of volumetric CLSM biofilm images. *J. Microbiol. Methods* 70, 424–433.
- Zunino, P., Geymonat, L., Allen, A.G., Legnani-Fajardo, C., Maskell, D.J., 2000. Virulence of a *Proteus mirabilis* ATF isogenic mutant is not impaired in a mouse model of ascending urinary tract infection. *FEMS Immunol. Med. Microbiol.* 29, 137–144.
- Zunino, P., Geymonat, L., Allen, A.G., Preston, A., Sosa, V., Maskell, D.J., 2001. New aspects of the role of MR/P fimbriae in *Proteus mirabilis* urinary tract infection. *FEMS Immunol. Med. Microbiol.* 31, 113–120.
- Zunino, P., Sosa, V., Allen, A.G., Preston, A., Schlapp, G., Maskell, D.J., 2003. *Proteus mirabilis* fimbriae (PMF) are important for both bladder and kidney colonization in mice. *Microbiology* 149 (Pt 11), 3231–3237.